Dissection of Malonyl-Coenzyme A Decarboxylation from Polyketide Formation in the Reaction Mechanism of a Plant Polyketide Synthase†

Joseph M. Jez, Jean-Luc Ferrer,‡ Marianne E. Bowman, Richard A. Dixon,§ and Joseph P. Noel*

Structural Biology Laboratory, The Salk Institute for Biological Studies, 10010 North Torrey Pines Road, La Jolla, California 92037, and Plant Biology Division, Samuel Roberts Noble Foundation, P.O. Box 2180, Ardmore, Oklahoma 73402

Received June 29, 1999; Revised Manuscript Received October 21, 1999

ABSTRACT: Chalcone synthase (CHS) catalyzes formation of the phenylpropanoid chalcone from one *p*-coumaroyl-CoA and three malonyl-coenzyme A (CoA) thioesters. The three-dimensional structure of CHS [Ferrer, J.-L., Jez, J. M., Bowman, M. E., Dixon, R. A., and Noel, J. P. (1999) *Nat. Struct. Biol. 6*, 775−784] suggests that four residues (Cys164, Phe215, His303, and Asn336) participate in the multiple decarboxylation and condensation reactions catalyzed by this enzyme. Here, we functionally characterize 16 point mutants of these residues for chalcone production, malonyl-CoA decarboxylation, and the ability to bind CoA and acetyl-CoA. Our results confirm Cys164's role as the active-site nucleophile in polyketide formation and elucidate the importance of His303 and Asn336 in the malonyl-CoA decarboxylation reaction. We suggest that Phe215 may help orient substrates at the active site during elongation of the polyketide intermediate. To better understand the structure−function relationships in some of these mutants, we also determined the crystal structures of the CHS C164A, H303Q, and N336A mutants refined to 1.69, 2.0, and 2.15 Å resolution, respectively. The structure of the C164A mutant reveals that the proposed oxyanion hole formed by His303 and Asn336 remains undisturbed, allowing this mutant to catalyze malonyl-CoA decarboxylation without chalcone formation. The structures of the H303Q and N336A mutants support the importance of His303 and Asn336 in polarizing the thioester carbonyl of malonyl-CoA during the decarboxylation reaction. In addition, both of these residues may also participate in stabilizing the tetrahedral transition state during polyketide elongation. Conservation of the catalytic functions of the active-site residues may occur across a wide variety of condensing enzymes, including other polyketide and fatty acid synthases.

The polyketides produced by bacteria, fungi, and plants offer a rich source of biologically active compounds of pharmacological interest. Many of the polyketide synthases are large assemblies of multifunctional or monofunctional proteins (*1*, *2*). For example, 6-deoxyerythronolide B synthase, a modular polyketide synthase, functions as a complex of multifunctional proteins that use a different active site for each catalytic step, and shuttle substrates between active sites via acyl carrier proteins (*3*). However, the plant polyketide synthases, including chalcone synthase (CHS)[1] and stilbene synthase (STS), function as dimeric proteins (monomer size of 42−45 kDa) that do not use acyl carrier proteins but act directly on coenzyme A (CoA)-thioesters of carboxylic acids (*4*, *5*). Also, unlike the larger polyketide synthases, CHS and related proteins use a single active site to perform a series of decarboxylation, condensation, cyclization, and aromatization reactions (*5*−*7*).

As a pivotal enzyme in the flavonoid branch of the phenylpropanoid biosynthetic pathway, CHS supplies 4,2′,4′,6′-tetrahydroxychalcone (chalcone) to an array of downstream enzymes that produce anthocyanin pigments, anti-microbial phytoalexins, and flavonoid inducers of *Rhizobium* nodulation genes (*8*−*10*). The natural products produced by this pathway are of interest as potential cancer chemopreventive and pharmacological agents (*11*−*15*) and are constituents in plant-rich diets associated with a reduced incidence of cardiovascular disease and some forms of cancer (*16*, *17*).

Mechanistically, CHS orchestrates the condensation of one *p*-coumaroyl-CoA and three malonyl-CoA molecules into chalcone (*18*) (Figure 1a). The reaction begins with the transfer of a *p*-coumaroyl-moiety from the CoA-linked starter molecule to Cys164 at the active site (*6*−*7*, *19*). Next, the sequential condensation of three acetate units derived from three malonyl-CoA molecules with the enzyme-bound coumaroyl moiety forms a tetraketide intermediate. Inherent in

† This work was supported by funds from the Samuel Roberts Noble Foundation and the Salk Institute to J.P.N. J.M.J. is an NIH Postdoctoral Research Fellow (CA80396) and also received financial support from the Hoffman Foundation Pioneer Fund. A preliminary account of this study was presented at the American Society for Biochemistry and Molecular Biology meeting in San Francisco, CA, May 16−20, 1999.

* To whom correspondence should be addressed at The Salk Institute for Biological Studies. Phone: (858) 453-4100, ext. 1442. Fax: (858) 452-3683. E-mail: noel@sbl.salk.edu.

‡ Permanent address: IBS/LCCP, 41 rue Jules Horowitz, 38027 Grenoble cedex 1, France.

§ Plant Biology Division.

[1] Abbreviations:ACS, acridone synthase; BBS, bibenzyl synthase; chalcone, 4,2′,4′,6′-tetrahydroxychalcone; CHI, chalcone isomerase (EC 5.5.1.6); CHS, chalcone synthase (EC 2.3.1.74); CoA, coenzyme A; DTT, D/L-dithiothreitol; KAS, *β*-ketoacyl synthase; naringenin, 5,7,4′-trihydroxyflavanone; PCR, polymerase chain reaction; 2-PS, 2-pyrone synthase; STS, stilbene synthase; TLC, thin-layer chromatography.

10.1021/bi991489f CCC: $19.00
Published on Web 01/12/2000

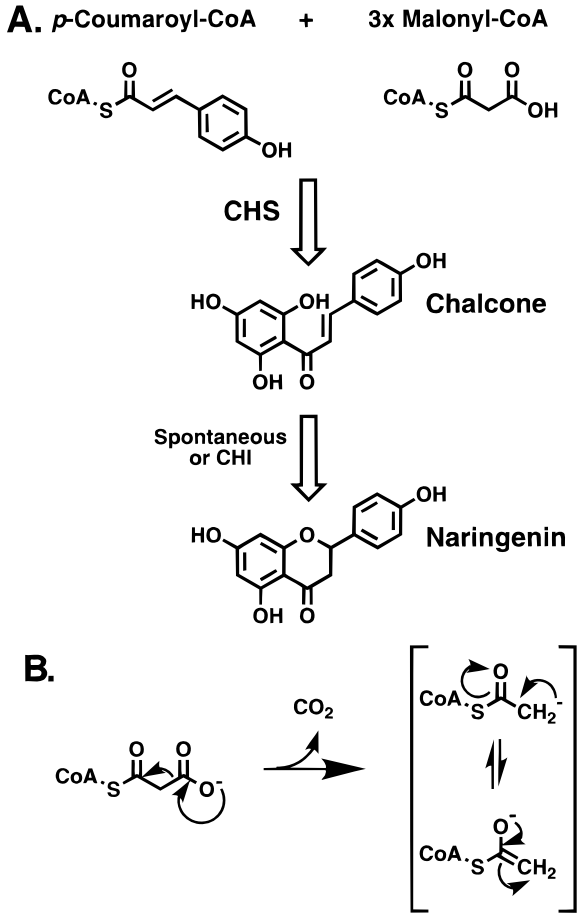

FIGURE 1: Reactions catalyzed by CHS. (A) The overall reaction catalyzed by CHS produces chalcone, which spontaneously cyclizes in a nonstereospecific manner in solution or stereospecifically via CHI to form naringenin. (B) The decarboxylation reaction catalyzed by CHS produces a resonance-stabilized carbanion intermediate utilized during polyketide elongation.

the condensation reaction is decarboxylation of malonyl-CoA to an acetyl-CoA carbanion that serves as a nucleophile during the chain extension reactions (Figure 1B) (*20*). The tetraketide intermediate then cyclizes by an intramolecular Claisen condensation into a hydroxylated aromatic ring system. In plants, chalcone isomerase (CHI) rapidly and stereospecifically converts chalcone to (−)(2*S*)-5,7,4′-trihydroxyflavanone (naringenin); however, in the absence of CHI, chalcone spontaneously forms mixed enantiomers of naringenin through a nonstereospecific ring closure in solution (*21*).

The crystal structure of CHS provides a view of the architecture supporting the chemistry of polyketide formation in plants (*22*). The overall fold of CHS (Figure 2a) resembles that of β-ketoacyl synthase (KAS) II (*23*) and thiolase (*24*). The structure of the CHS·CoA complex showed that the pantetheine arm of CoA presents substrates to a buried active-site cavity comprised of two distinct pockets. In the structures of CHS complexed with naringenin or resveratrol, the coumaroyl-derived portions of both molecules bind inside one of these pockets termed the coumaroyl-binding pocket. The other pocket, designated the cyclization pocket, is adjacent to the coumaroyl-binding site and the boundary of both regions approximately defined by the catalytic cysteine (*6*, *19*). Since the malonyl-derived portions of naringenin and resveratrol reside in this pocket, this site likely accommodates the elongating polyketide and is the location where cyclization of the tetraketide intermediate into a hydroxylated aromatic ring system occurs. Remarkably, few chemically reactive amino acids are present at this active site to catalyze a series of decarboxylation, condensation, cyclization, and aromatization reactions upon a continually changing set of intermediates. Four amino acids (Cys164, Phe215, His303, and Asn336) situated at the intersection of the CoA-binding site, the coumaroyl-binding site, and the cyclization pocket likely play essential and distinct roles during malonyl-CoA decarboxylation and chalcone formation (Figure 2B). These residues are conserved in the known CHS-related enzymes from plants (Figure 2C), including stilbene synthase [STS (*25*)], bibenzyl synthase [BBS (*26*)], acridone synthase [ACS (*27*)], and 2-pyrone synthase [2-PS (*28*)], and a number of bacterial CHS-like genes (*29*−*31*).

Overall, the functional and structural studies presented here establish the role of Cys164 as the nucleophile in the reaction and as the attachment site of the elongating polyketide intermediate. These studies also demonstrate that His303 and Asn336 serve as the catalytic machinery responsible for malonyl-CoA decarboxylation. Finally, the positional conservation of the CHS active-site residues with those of KAS II suggests that the roles of these residues are likely conserved in other polyketide and fatty acid synthases.

EXPERIMENTAL PROCEDURES

Materials. Alfalfa (*Medicago sativa*) *CHS2* was cloned in the lab of R.A.D. (*32*). The pET-28a(+) expression vector and *Escherichia coli* strain BL21(DE3) were purchased from Novagen. All oligonucleotides were ordered from Operon, Inc. NuSieve GTG agarose was obtained from FMC BioProducts. Restriction endonucleases, T4 DNA ligase, and dNTPs were from New England Biolabs. The QuikChange polymerase chain reaction (PCR)-based site-directed mutagenesis kit was from Stratagene. Ni^{2+}-NTA was bought from Qiagen. Benzamidine-Sepharose and the Superdex-200 FPLC column were from Pharmacia. The [2-^{14}C]malonyl-CoA (45.8 mCi/mmol) and [^{14}C]acetyl-CoA (53.0 mCi/mmol) were purchased from NEN and Amersham, respectively. Thrombin, naringenin, CoA, acetyl-CoA, and malonyl-CoA were purchased from Sigma. Reagents for the synthesis of *p*-coumaroyl-CoA were purchased from Aldrich or Sigma.

Construction of the pHIS8-CHS Expression Vector and Site-Directed Mutagenesis. A set of three sense (5′-dCATGAAACACCACCACCACCAC-3′, 5′-dCACCACCACGGTGGTCTG-3′, and 5′-dGTTCCGCGTGGTTCCCATGGCG-3′) and three antisense (5′-dGATCCGCCATGGGAACCACG-3′, 5′-dCGGAACCAGACCACCGTG-3′, and 5′-dGTGCTGGTGGTGGTGGTGGTGTTT-3′) overlapping oligonucleotides were used to introduce an *Nco*I site after the thrombin cleavage site of pET-28a(+) and to extend the N-terminal hexahistidyl-coding sequence to eight histidines (Figure 3a). The new sequence uses *E. coli*-preferred codons and an AAA codon at the +2 site. The second and third sense and the second and third anti-sense strands were phosphorylated using T4 polynucleotide kinase, followed by incubation of all six oligonucleotides with T4 ligase. The 62 bp fragment was isolated from a 3% NuSieve GTG agarose gel. pET-28a(+) was cut with *Nde*I and *Bam*HI, and the resulting 5279 bp product gel purified. The synthetic 62

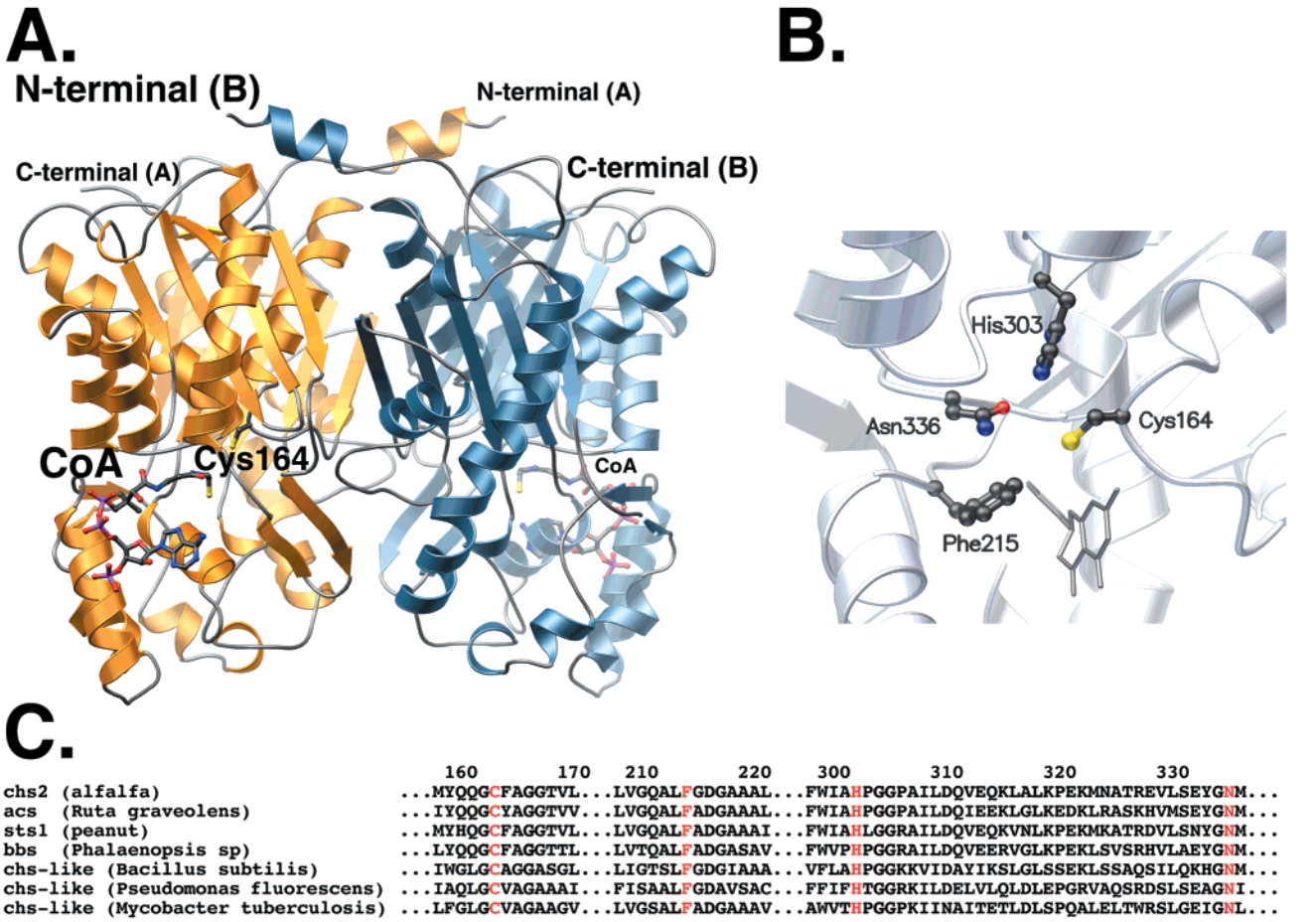

FIGURE 2: Overall fold of CHS and the active site. (A) Ribbon trace of the CHS N336A dimer (monomer A in gold and monomer B in blue) complexed with CoA highlights the location of the active site relative to the location of bound CoA. Cys164 and CoA are shown as ball-and-stick models with the N- and C-termini of each monomer indicated. (B) The four active site residues are shown in ball-and-stick with the location of naringenin indicated by a stick drawing. (C) Sequence alignment of the active sites of CHS-related enzymes. The four conserved active site residues are highlighted in red. Figure prepared using MOLSCRIPT (*85*) and rendered with POV-Ray (*86*).

bp fragment was then ligated into the *Nde*I/*Bam*HI-digested pET-28a(+). Automated nucleotide sequencing (Salk Institute DNA sequencing facility) verified the sequence of the pHIS8 construct. The alfalfa *CHS2* gene was amplified by PCR using 5′-dCGCGTGGTTCCCATGGC**ATG**GTGAGTGTGTCTGAAATT-3′ as the forward primer (*Nco*I site underlined and the translation start site in bold), 5′-dGCTCGAATTCGGATCC**TCA**TATAGCCACGCTACG-3′ as the reverse primer (*Bam*HI site underlined and the stop codon in bold), and pBluescript as template. The 1.2 kb PCR product was digested with *Nco*I and *Bam*HI, gel purified, and ligated with *Nco*I/*Bam*HI-digested pHIS8 to generate the expression vector. All site-directed mutants were constructed using the QuikChange (Stratagene) PCR method. Either single primers or a mixture of oligonucleotide primers were used (Table 1). Automated nucleotide sequencing confirmed the fidelity of the PCR products (Salk Institute DNA sequencing facility).

Expression and Purification. Constructs of pHIS8-CHS (wild-type and mutants) were transformed into *E. coli* BL21-(DE3). Transformed *E. coli* were grown at 37 °C in Terrific broth containing 50 μg/mL kanamycin until $A_{600nm} = 1.2$. After induction with 0.5 mM isopropyl 1-thio-β-D-galactopyranoside, the cultures were grown at 20 °C for 4 h. Cells were pelleted, harvested, and resuspended in 50 mM Tris-HCl (pH 8.0), 500 mM NaCl, 20 mM imidazole (pH 8.0), 20 mM β-mercaptoethanol, 10% (v/v) glycerol, and 1% (v/v) Tween-20. After sonication and centrifugation, the supernatant was passed over a Ni^{2+}-NTA column, the column was washed with 10 bed volumes of lysis buffer and 10 bed volumes of lysis buffer minus Tween-20, and then the His8-tagged protein was eluted with lysis buffer minus Tween-20 but containing 250 mM imidazole (pH 8.0). Incubation with thrombin during dialysis for 24 h at 4 °C against the lysis buffer without Tween-20 removed the amino-terminal His8-tag. Dialyzed protein was reloaded on a Ni^{2+}-NTA column and the flow-through depleted of thrombin using a benzamidine-Sepharose column. Gel filtration on a Superdex-200 FPLC column equilibrated with 25 mM Hepes (pH 7.5), 100 mM NaCl, and 5 mM dithiothreitol (DTT) was the final step. Fractions containing CHS were pooled, concentrated to 25 mg/mL, and stored at −80 °C in 5 mM Hepes (pH 7.5), 25 mM NaCl, and 5 mM DTT after buffer exchange.

Synthesis of p-Coumaroyl-CoA. The two-step synthesis of coumaroyl-CoA involved generation of the *N*-hydroxysuccinimide ester of 4-coumaric acid followed by a thioester exchange with CoA as originally described by Stoeckigt and Zenk (*33*).

Chalcone Synthase Assay. CHS activity was determined by measuring the conversion of *p*-coumaroyl-CoA and [2-^{14}C]malonyl-CoA into reaction products (*18*). The standard assay conditions contained 100 mM potassium phos-

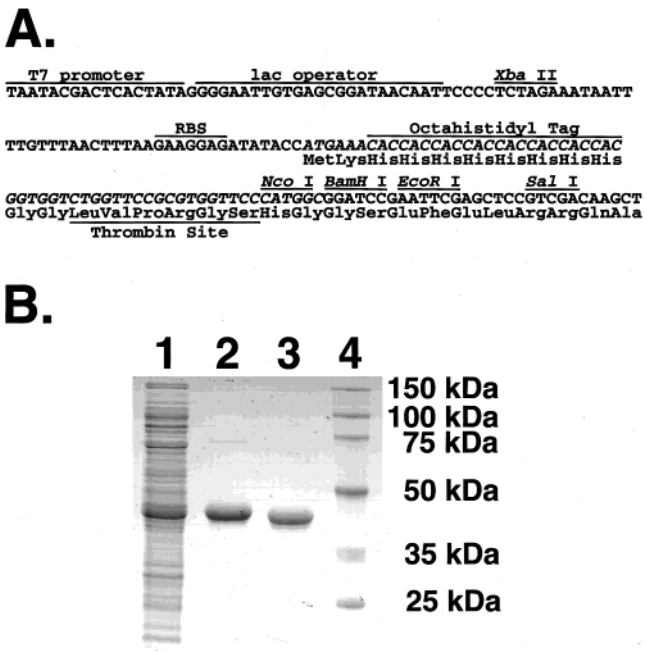

FIGURE 3: Expression and purification. (A) Sequence of the pHIS8 vector. Portions retained from pET-28a(+) are in regular type with the newly constructed sequences shown in italics. The start of the T7 promoter is at 370 bp in the pET-28a(+) vector. (B) SDS−PAGE of CHS purification. Samples were stained for total protein using Coomassie Blue. Lane 1, 50 μg of sonicate; lane 2, 3 μg of Ni^{2+}-NTA purified CHS (before thrombin digest); lane 3, 3 μg of gel filtration purified CHS (after thrombin digest); lane 4, molecular mass markers (masses indicated on gel).

phate buffer (pH 7.0), 15 μM *p*-coumaroyl-CoA, and 30 μM malonyl-CoA (50 000 cpm) in a 100 μL reaction volume at 25 °C. Reactions were quenched with ethyl acetate. Extracts were evaporated to dryness, redissolved in methanol, and applied to Whatman LK6D silica TLC plates. Chromatograms were developed in chloroform:methanol:water (65:25:4, v/v/v). The position of naringenin chalcone was visualized by autoradiography and by comparison with an authentic standard (R_f = 0.70). Products were quantitated by scraping sections of the TLC plate into Ecolume scintillation fluid, detecting ^{14}C-radioactivity with a scintillation counter, and converting the corrected cpm into nmoles of product using the final specific radioactivity of [^{14}C]malonyl-CoA. Activity was defined by incorporation of one *p*-coumaroyl-CoA into naringenin. Kinetic constants were determined from initial velocity measurements, in which product formation was linear over the time periods monitored (up to 2 h for low activity mutants), using the standard assay conditions with either 500 μM malonyl-CoA (50 000 cpm) and varied *p*-coumaroyl-CoA concentrations (0.5−180 μM) or 180 μM *p*-coumaroyl-CoA and varied malonyl-CoA concentrations (2.2−500 μM; 10000−50000 cpm).

Chalcone Synthase Decarboxylation Assay. Measurement of the decarboxylation activity of CHS used a radiometric assay that monitored conversion of [^{14}C]malonyl-CoA to [^{14}C]acetyl-CoA (*34*). Assays contained 100 mM potassium phosphate buffer (pH 7.0) and 30 μM malonyl-CoA (50 000 cpm) in a 50 μL reaction volume at 25 °C. Reactions were quenched with acetic acid and applied to Whatman LK6D TLC plates. The separation of [^{14}C]malonyl-CoA (R_f = 0.24) and [^{14}C]acetyl-CoA (R_f = 0.62) was carried out in 2-propanol:ammonium hydroxide:water (80:13:5, v/v/v) with product quantitation as described above. Kinetic constants for the decarboxylation of malonyl-CoA were determined from initial velocity measurements, in which product formation was linear over the time periods monitored, using the standard assay conditions with varied malonyl-CoA (2.2−422 μM or 2.2−844 μM; 10000−50000 cpm).

Intrinsic Fluorescence Titration. Binding of CoA and acetyl-CoA to CHS was measured by monitoring the change of fluorescence in CHS upon ligand binding. Measurements were made on a PTI−Alphascan (Photon Technologies International) fluorimeter (excitation λ_{max} = 280 nm and emission λ_{max} = 330 nm). Titrations were performed at 25 °C by addition of CoA or acetyl-CoA to 0.5 mL of 100 mM potassium phosphate (pH 7.0) and 1 mM EDTA containing 4 μg of protein (0.1 μM protein) until the emission signal did not undergo further change. Control titrations of CHS with buffer alone did not change the intrinsic fluorescence over the entire volume range used. Likewise, addition of ligands to buffer alone did not produce any fluorescence change. The K_d values for CoA and acetyl-CoA binding were calculated by nonlinear least squares iterative curve fitting using Kaleidagraph (Abelbeck Software). The data were fit to a reversible two-state model of binding (eq 1), where

$$\Delta F = (\Delta F_{max}[L])/([L] + K_d) \quad (1)$$

ΔF is the change in fluorescence observed in the presence of CoA or acetyl-CoA at a concentration, [L], and ΔF_{max} is the maximal change in fluorescence (*35*). The data were also plotted as a linear transform of the same equation in which the slope yields K_d (*R* versus *R*/[L]), where *R* represents the change in fluorescence when ligand is added.

Crystallography. Crystals of the C164A, H303Q, and N336A CHS mutants were grown by vapor diffusion in hanging drops of 1:1 mixture of protein and crystallization buffer (2.2−2.4 M ammonium sulfate, 0.1 M bis-Tris-propane, pH 6.5, and 2 mM DTT) at 4 °C. Crystals of the C164A and N336A mutants were isomorphous with those obtained for wild-type CHS and grew in space group $P3_221$ with a single monomer in the asymmetric unit and unit cell dimensions of $a = b$ = 97.36 Å and c = 65.20 Å for the C164A mutant and $a = b$ = 97.40 Å and c = 65.20 Å for the N336A mutant. Crystals of the H303Q mutant were isomorphous with those obtained for the previously described C164S mutant and grew in space group $P3_121$ with unit cell dimensions of $a = b$ = 97.86 Å and c = 129.6 Å and two monomers per asymmetric unit. Crystals of the N336A mutant were stabilized in 40% (v/v) PEG400, 50 mM bis-Tris-propane (pH 6.5), and 50 mM ammonium sulfate containing 5 mM CoA. The same stabilizer minus CoA was used for crystals of the other mutants. Diffraction data were collected for each mutant from a single-crystal mounted in a cryoloop and flash frozen in a nitrogen stream at 105 K using a DIP2030 imaging plate system (Mac-Science Corporation) and CuKα radiation produced by a rotating anode operated at 45 kV and 100 mA and equipped with double focusing Pt/Ni coated mirrors. All images were indexed and integrated using DENZO and the reflections merged with SCALEPACK (*36*). Data reduction was completed using programs in CCP4 (*37*) (Table 2).

Structures were determined by the difference Fourier method (*38*, *39*). Wild-type CHS minus the side-chain atoms

Table 1: Oligonucleotide Primers for Site-Directed Mutagenesis[a]

C164(A/S)	5′-dATGATGTACCAACAAGGG(G/T)CTTTTGCAGGTGGCACGGTG-3′
C164D	5′-dATGATGTACCAACAAGGGGATTTTGCAGGTGGCACGGTG-3′
F215(S/Y)	5′-dGTTGGACAAGCACTAT(A/C)TGGAGATGGAGCTGCTG-3′
F215W	5′-dGTTGGACAAGCACTATGGGGGAGATGGAGCTGCTG-3′
H303(D/T/N/A)	5′-dCTCAATCTTTTGGATTGCA(G/A)(C/A)TCCTGGTGGACCTGCAATT-3′
H303Q	5′-dTCAATCTTTTGGATTGCACAGCCTGGTGGACCTGCAATTC-3′
N336(D/H/A)	5′-dGTGCTAAGTGAATATGGA(C/G)(C/A)TATGTCAAGTTCAGCA-3′
N336(Q/K)	5′-dGTGCTAAGTGAATATGGA(C/A)A(A/G)ATGTCAAGTTCAAGT-3′

[a] Codons encoding the mutations are underlined.

Table 2: Data Collection and Refinement Statistics for the CHS C164A, H303Q, and N336A Mutant Structures

	C164A	H303Q	N336A
max. resolution (Å)	1.69	2.00	2.15
total reflections/unique reflections	88359/39526	168254/45654	49636/18202
completeness of data (highest shell) (%)	97.0 (83.2)	93.0 (87.8)	91.9 (90.5)
I/σ (highest shell)	18.8 (7.4)	6.3 (1.7)	9.1 (2.4)
R_{sym} (highest shell)[a]	0.026 (0.089)	0.068 (0.390)	0.056 (0.303)
R-factor[b] (%)	17.0	19.9	17.9
$R_{free-factor}$[c] (%)	20.1	26.7	25.7
no. of protein atoms	2994	5956	2979
no. of ligand atoms	24 (5 sulfate and 19 buffer)	10 (sulfate)	53 (5 sulfate and 48 CoA)
no. of water molecules	365	326	189
rms deviation from ideal bond lengths (Å)	0.009	0.015	0.015
rms deviation from ideal bond angles (deg)	2.1	3.1	3.0
average *B*-factor, protein (Å^2)	17.5	28.1	33.7
average *B*-factor, sulfate/ligand (Å^2)	27.4/32.4	39.4/−	53.7/44.7
average *B*-factor, solvent (Å^2)	26.3	30.2	38.3

[a] $R_{sym} = \sum|I_h - \langle I_h\rangle|/\sum I_h$, where $\langle I_h\rangle$ is the average intensity over symmetry equivalent reflections. [b] *R*-factor $= \sum|F_{obs} - F_{calc}|/\sum F_{obs}$, where summation is over the data used for refinement. [c] R_{free}-factor is the same definition as for *R*-factor, but includes only 5% of data excluded from refinement (*84*).

corresponding to the mutated residue and all solvent atoms comprised the starting model. The protein model was refined using REFMAC (*40*) and ARP (*41*). During refinement, structure factors obtained from intensity data were used to generate $|2F_o - F_c|$ and $|F_o - F_c|$ electron density maps with phases calculated from the structure of the in-progress model. Inspection of the electron density maps and model building were performed with O (*42*). After an initial round of refinement, the difference density maps clearly showed the introduced mutations and enabled the mutated side chains to be incorporated into each structural model. At this stage, density for CoA was apparent in the N336A mutant model and the ligand was fit into the density. Water molecules introduced by ARP were examined using $|2F_o - F_c|$ and $|F_o - F_c|$ maps and were included in the final models if their peak heights were greater than 2.0σ, if they were within hydrogen-bonding distance of appropriate protein or solvent atoms, and if they refined with thermal *B*-factors of ≤ 60 Å^2. Successive iterations of refinement using REFMAC/ARP and model building in O were performed with refinement converging to the final *R*-factors shown in Table 2. Model quality was checked with PROCHECK (*43*). Atomic coordinates and structure factors for the CHS C164A, H303Q, and N336A mutant structures have been deposited in the Protein Data Bank as 1D6F, 1D6I, and 1D6H, respectively.

RESULTS

Expression and Purification of Recombinant Wild-Type and CHS Mutants. Single point mutants of Cys164, Phe215, His303, and Asn336 were generated to evaluate the role of each active-site residue in the reaction mechanism. Wild-type and mutant CHSs were overexpressed in *E. coli* as His8-tagged proteins and purified to homogeneity using Ni^{2+}-affinity and gel filtration chromatography (Figure 3B). Purified wild-type CHS and the mutants had the same mobility on SDS−PAGE (not shown) and migrated with a monomer molecular weight of approximately 40 kDa. Likewise, wild-type CHS and all the mutant proteins eluted from the gel filtration column as an 80−85 kDa species representing the physiological dimer. One liter cultures of each CHS form typically yielded 10−20 mg of pure protein.

Activity Screen for Naringenin Formation and Malonyl-CoA Decarboxylation. Wild-type CHS and the mutants were assayed for naringenin formation (Figure 4). Only the H303Q mutant retained a high level of activity compared to wild-type CHS. Naringenin formation occurred in the F215S, F215Y, F215W, N336A, N336D, and N336K mutants at greatly reduced rates. Wild-type CHS and the mutant enzymes also produced lesser quantities of compounds corresponding to the addition of fewer than three acetate units to coumaroyl-CoA. While these truncated products have not been unequivocally identified, they likely include benzalacetone, dihydropyrone, and styrylpyrone (*44*, *45*). In wild-type CHS and the H303Q, N336D, and N336K mutants, naringenin accounted for more than 95% of the observed products. For the F215S, F215Y, F215W, and N336A mutants, naringenin formation accounted for 28%, 65%, 35%, and 53% of the final products, respectively. The C164S, C164A, C164D, H303A, H303N, H303D, H303T, N336Q, and N336H mutants had no detectable activity in assays using 100 μg of protein for 2 h.

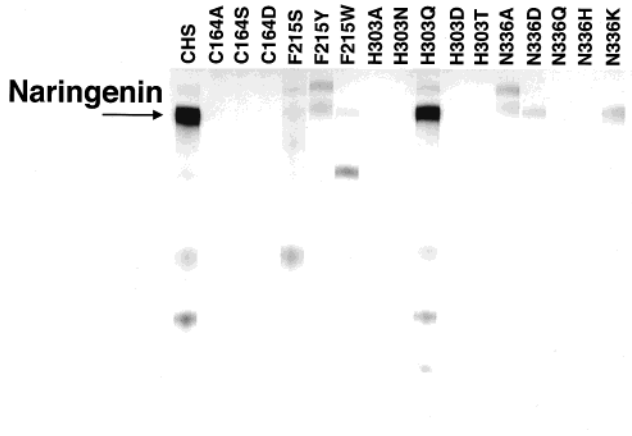

FIGURE 4: TLC of reaction product formation by wild-type and mutant CHSs. Using the conditions for the standard CHS assay, 50 μg of each protein was incubated for 30 min with coumaroyl- and [^{14}C]malonyl-CoA to obtain a profile of the reaction products for each mutant. The position of authentic naringenin standard is indicated.

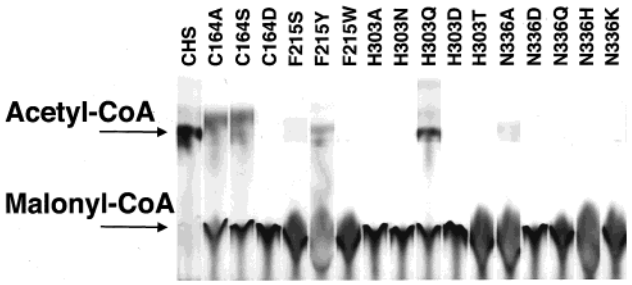

FIGURE 5: TLC of the decarboxylation of [^{14}C]malonyl-CoA to [^{14}C]acetyl-CoA by wild-type and mutant CHSs. Assay conditions were as described in the Experimental Procedures. A total of 50 μg of each protein was incubated for 30 min at room temperature with [^{14}C]malonyl-CoA. The positions of authentic [^{14}C]malonyl-CoA and [^{14}C]acetyl-CoA are as indicated.

As expected, the mutants capable of forming naringenin also decarboxylated [^{14}C]malonyl-CoA to [^{14}C]acetyl-CoA (Figure 5). Decarboxylation activity was absent in the C164D, H303A, H303N, H303D, H303T, N336Q, and N336H mutants, even when assayed with 100 μg of protein for 2 h. Surprisingly, the C164S and C164A mutants retained relatively high decarboxylation activity. This result suggests that His303 and Asn336 catalyze the decarboxylation of malonyl-CoA.

Finally, assays of wild-type and mutant CHS enzymes in the presence of coumaroyl-CoA, but with [^{14}C]acetyl-CoA replacing [^{14}C]malonyl-CoA, showed that product formation did not occur (data not shown). This experiment confirmed that the acetyl-CoA carbanion required for the condensation reaction is derived from decarboxylation of malonyl-CoA and that, unlike in thiolase (*46*), the CHS active site does not contain a general base that can activate acetyl-CoA.

Steady-State Kinetic Parameters for Naringenin Formation. To examine the contribution of Cys164, Phe215, His303, and Asn336 to naringenin formation, steady-state kinetic parameters for wild-type CHS and the active mutants were determined. The kinetic parameters of alfalfa CHS2 for *p*-coumaroyl-CoA and malonyl-CoA (Table 2) were similar to those reported for CHS and STS from other sources (*5*, *6*, *47*−*49*). The role of Cys164 as the nucleophile and attachment site for the polyketide intermediate was confirmed by the lack of activity in the C164S, C164A, and C164D mutants.

Table 3: CHS Steady-State Kinetic Parameters[a]

	k_{cat} ($\times 10^{-3}$ min^{-1})	K_m (μM)	k_{cat}/K_m (s^{-1} M^{-1})
	p-Coumaroyl-CoA		
WT	2210 ± 108	4.5 ± 0.7	8190
F215S	24.1 ± 2.8	3.8 ± 0.8	106
F215Y	38.8 ± 3.7	18.3 ± 3.3	35.3
F215W	20.4 ± 0.8	30.4 ± 3.5	11.1
H303Q	289 ± 19	7.6 ± 1.7	634
N336A	31.7 ± 2.3	5.8 ± 0.7	91.0
N336D	1.3 ± 0.1	18.3 ± 1.7	1.2
N336K	0.7 ± 0.1	28.1 ± 4.2	0.4
	Malonyl-CoA		
WT	3710 ± 210	4.1 ± 1.0	15 080
F215S	37.5 ± 2.9	104 ± 21	6.0
F215Y	20.1 ± 2.5	184 ± 28	1.8
F215W	13.5 ± 0.4	107 ± 9	2.1
H303Q	556 ± 20	8.2 ± 1.1	1130
N336A	7.9 ± 0.6	41.9 ± 3.7	3.1
N336D	0.7 ± 0.1	33.2 ± 5.2	0.3
N336K	2.6 ± 0.3	127 ± 36	0.3

[a] All reactions were performed using the radiometric assay in potassium phosphate buffer (pH 7.0) as described in the Experimental Procedures. All k_{cat} and K_m values were determined using Kaleidagraph and are expressed as a mean ± SE for an $n = 3$.

Of the His303 mutants, only the H303Q mutant remained active for naringenin formation with a modest 10-fold decrease in k_{cat}/K_m for both coumaroyl-CoA and malonyl-CoA that primarily results from a decreased turnover rate. Significantly, this result indicates that His303 does not function as a general base during formation of the Cys164 thiolate anion. Substitutions of Asn336 produced inactive (N336Q and N336H) and impaired enzymes (N336A, N336D, and N336K). The N336A mutant exhibited a 90-fold decrease in k_{cat}/K_m for coumaroyl-CoA and a 4900-fold decrease in k_{cat}/K_m for malonyl-CoA. Both the N336D and N336K mutants possessed drastically reduced k_{cat}/K_m for naringenin formation using both substrates. Each of the Phe215 mutants exhibited 80−750-fold decreases in k_{cat}/K_m for coumaroyl-CoA but 2500−8400-fold decreases in k_{cat}/K_m for malonyl-CoA. It should be noted that the N336A, F215S, F215Y, and F215W mutants are actually more effective catalysts than the values in Table 3 indicate, since these mutants generally make a higher percentage of truncated reaction products than of naringenin, by way of chalcone.

Steady-State Kinetic Parameters for Malonyl-CoA Decarboxylation. To further investigate the reaction mechanism of CHS, the steady-state kinetic parameters for malonyl-CoA decarboxylation in wild-type CHS and the mutants active for this reaction were determined (Table 4). Generally, the K_m values for the decarboxylation reactions catalyzed by wild-type CHS and the mutants are greater than the K_m values determined for naringenin formation. Likewise, the k_{cat} values for malonyl-CoA decarboxylation were slightly higher than those for naringenin formation. Since malonyl-CoA binds a different enzyme species in the decarboxylation assay than in the naringenin formation assay, i.e., CHS with a polyketide intermediate at Cys164, these differences were not unexpected. Similar rates to those of CHS for malonyl-CoA decarboxylation have been reported for grapevine STS (*6*).

Table 4: Malonyl-CoA Decarboxylation Steady-State Kinetic Parameters[a]

	k_{cat} ($\times 10^{-3}$ min^{-1})	K_m (μM)	k_{cat}/K_m (s^{-1} M^{-1})
WT	4090 ± 162	19.1 ± 2.7	3570
C164A	415 ± 14	18.5 ± 2.2	374
C164S	403 ± 14	23.0 ± 2.6	292
F215S	74.8 ± 2.4	54.6 ± 6.4	22.8
F215Y	171 ± 9	63.6 ± 9.2	44.8
F215W	49.3 ± 2.7	124 ± 14	7.9
H303Q	658 ± 20	25.2 ± 2.5	435
N336A	28.9 ± 1.6	67.8 ± 6.3	7.1
N336D	13.9 ± 0.8	159 ± 19	1.5
N336K	13.5 ± 1.7	339 ± 37	0.7

[a] All reactions were performed using the radiometric assay in potassium phosphate buffer (pH 7.0) as described in the Experimental Procedures. All k_{cat} and K_m values were determined using Kaleidagraph and are expressed as a mean ± SE for an $n = 3$.

In CHS, mutation of Cys164 to serine or alanaine yielded 10-fold reductions in k_{cat} for malonyl-CoA decarboxylation. Importantly, the C164A and C164S mutants demonstrate that Cys164 is not essential for the decarboxylation reaction. The C164D mutant eliminated the ability to decarboxylate malonyl-CoA, presumably because the presence of a carboxylate at the active site compromises the stability of the acetyl-CoA carbanion intermediate. The effects of mutations of both His303 and Asn336 indicate that these residues catalyze the decarboxylation of malonyl-CoA. The N336Q and N336H mutant proteins, as well as all the substitutions of His303, except for the H303Q mutation, abolished decarboxylation activity. The H303Q mutant exhibited only an 8-fold reduction in k_{cat}/K_m, while the N336A, N336D, and N336K mutants exhibited 500−5100-fold reductions in the k_{cat}/K_m for malonyl-CoA decarboxylation. Finally, the Phe215 mutants retained decarboxylase activity with 80−450-fold reductions in k_{cat}/K_m for the decarboxylation reaction.

CoA and Acetyl-CoA Fluorescence Titrations. To determine if the inactive mutants possessed impaired CoA and acetyl-CoA binding activity, titration of the intrinsic protein fluorescence was employed to measure the affinity of the 16 CHS mutants for these ligands. Since acetyl-CoA is not a viable starter molecule for CHS (*38*), it provides a mimic for portions of the CoA substrates. Panels A and B of Figure 6 illustrate titration curves for wild-type CHS with increasing concentrations of CoA and acetyl-CoA, respectively. The K_d values determined from these curves for ligand binding to wild-type CHS were 82 nM for CoA and 70 nM for acetyl-CoA. Table 5 summarizes the same K_d values measured for the CHS mutants. Most of the mutants bound CoA with roughly the same K_d value as wild-type CHS, except for the F215W and N336K mutants. The increased K_d values for CoA and acetyl-CoA binding in these two mutants likely results from steric interference in the CoA binding tunnel, since the amino acid substitutions at positions 215 and 336 introduce significantly larger side chains at these positions. For acetyl-CoA binding, the Cys164 and His303 mutations did not dramatically affect the K_d values, indicating that these residues do not contribute to binding of CoA or acetyl-CoA. Likewise, the F215S and F215Y mutants also bound acetyl-CoA with only a small variation in the K_d as compared to wild-type CHS. However, all of the mutations of Asn336, except the N336H mutant, exhibited K_d values for binding acetyl-CoA that were 15−40-fold higher than wild-type CHS, suggesting that this residue contributes to substrate binding.

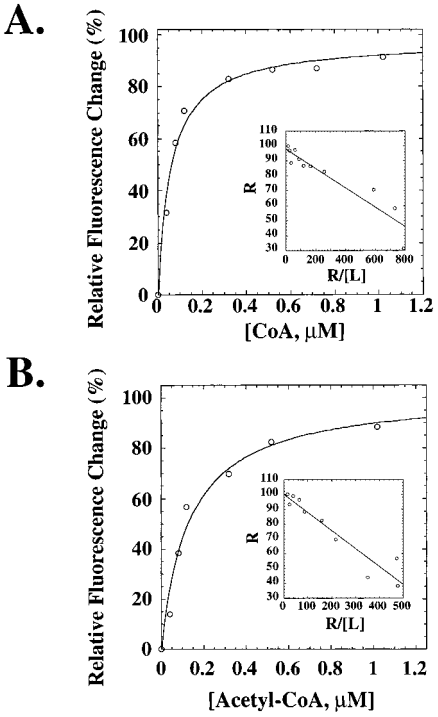

FIGURE 6: Measurement of the binding of CoA and acetyl-CoA to wild-type CHS. Binding of CoA (A) and acetyl-CoA (B) to CHS was determined by measuring the decrease in protein fluorescence emission at 330 nm (excitation at 280 nm) upon addition of ligand (0−2.1 μM) under conditions described in the Experimental Procedures. Only titration data from 0 to 1 μM is shown. Data are plotted as percentage of fluorescence change versus ligand concentration with K_d values determined as described. The inset graph shows a linear transformation of titration data (0−2.1 μM) where R is the change in fluorescence upon ligand addition.

Table 5: CoA and Acetyl-CoA Binding Constants

	CoA K_d (nM)[a]	acetyl-CoA K_d (nM)		CoA K_d (nM)[a]	acetyl-CoA K_d (nM)
WT	82 ± 16	70 ± 14	H303Q	112 ± 35	68 ± 20
C164A	57 ± 12	187 ± 47	H303D	60 ± 7	131 ± 17
C164S	73 ± 13	95 ± 17	H303T	135 ± 17	154 ± 25
C164D	88 ± 16	108 ± 19	N336A	128 ± 24	983 ± 112
F215S	69 ± 15	158 ± 33	N336D	65 ± 6	1100 ± 390
F215Y	60 ± 8	79 ± 12	N336Q	82 ± 14	2770 ± 240
F215W	50 900 ± 11 700	8080 ± 2350	N336H	47 ± 8	141 ± 26
H303A	160 ± 48	174 ± 35	N336K	22 800 ± 5200	10 100 ± 1100
H303N	71 ± 18	57 ± 9			

[a] K_d values were determined as described under the Experimental Procedures and are expressed as a mean ± SE for an $n = 3$.

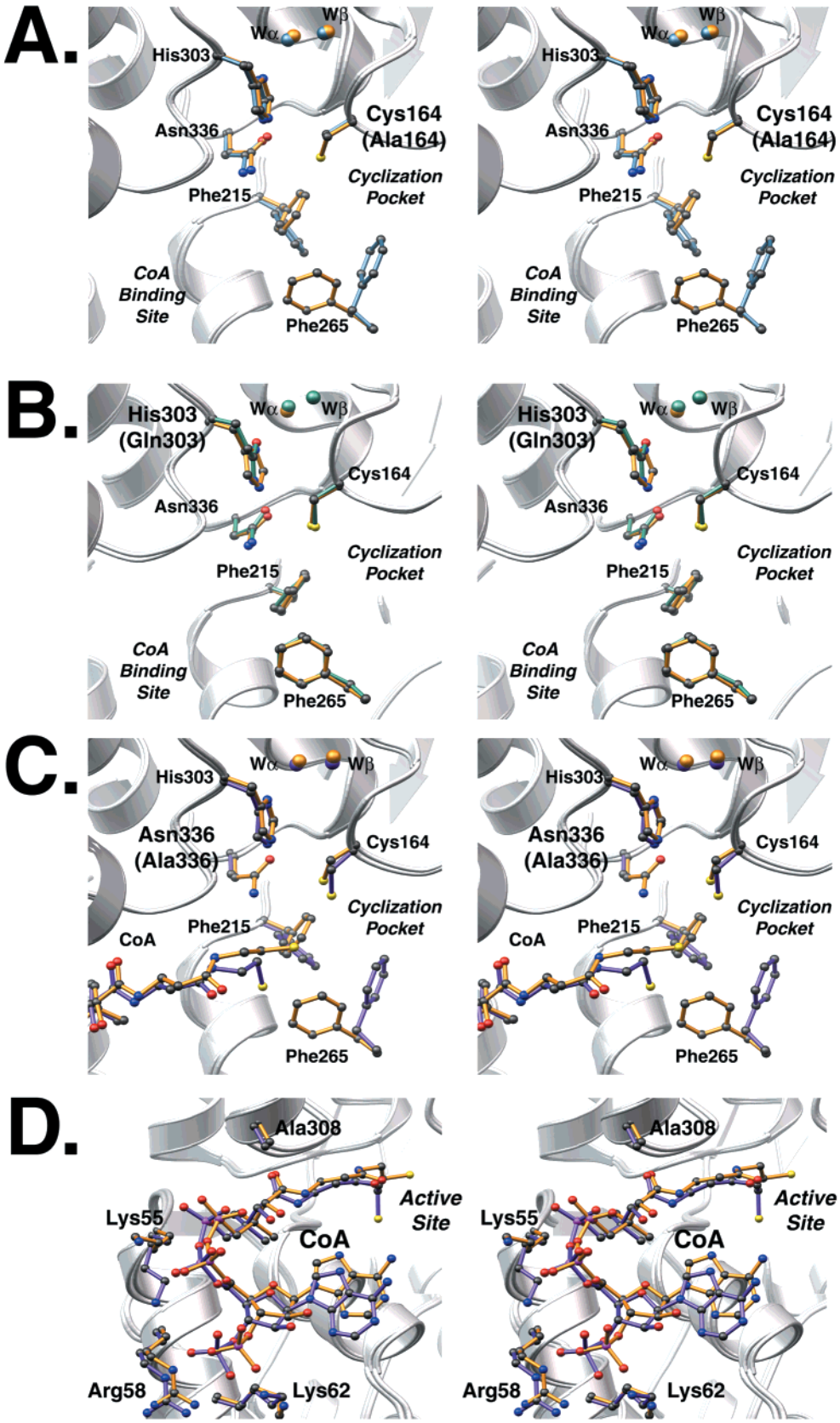

FIGURE 7: Structural comparison of wild-type CHS and mutants. (A) Superimposition of the active-site residues and two water molecules (W_α and W_β) of wild-type CHS (gold) and the C164A mutant (blue). Carbon, nitrogen, oxygen, and phosphorus atoms of the side chains and CoA are shown in black, blue, red, and pink, respectively. The bis-Tris propane molecule bound in the CoA tunnel of the C164A mutant is not shown for clarity. (B) Superimposition of the wild-type (gold) and H303Q mutant (cyan) active sites. (C) Superimposition of the wild-type (gold) and N336A mutant (purple) active sites, including the terminal portion of bound CoA. The relative locations of the cyclization pocket and the CoA binding tunnel are indicated in panels A−C, and the view is oriented as in Figure 2, panels A and B. (D) Comparison of the CoA binding sites in the wild-type (gold) and N336A mutant (purple). Figure prepared using MOLSCRIPT (*85*) and rendered with POV-Ray (*86*).

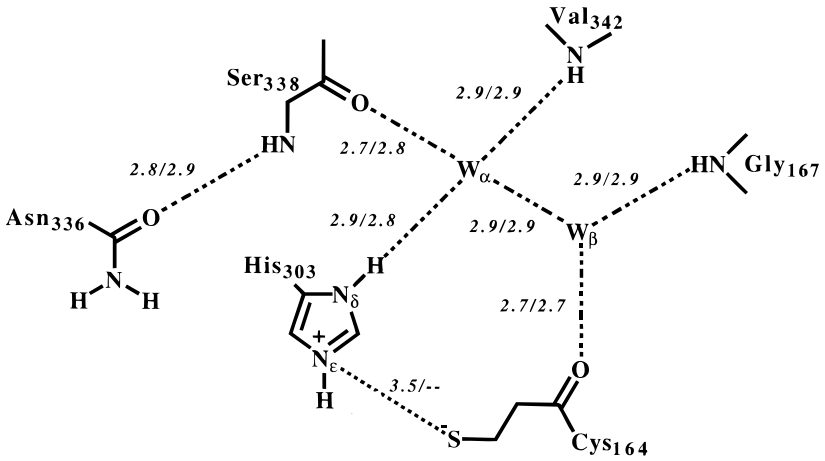

FIGURE 8: Schematic of the hydrogen bond network observed at the CHS active site. The first number is the distance in angstroms observed in the wild-type CHS structure and the second number the distance observed in the C164A mutant structure. Similar distances are maintained in the H303Q and N336A mutant structures.

The difference in K_d for CoA versus acetyl-CoA observed in the Asn336 mutants indicates a preference for ligands with a thioester carbonyl.

Structures of the CHS Mutants. The overall structures of the C164A, H303Q, and N336A mutants were nearly unchanged compared to wild-type CHS with rms deviations of the backbone atoms of 0.15, 0.21, and 0.18 Å, respectively. The overall fold of the N336A mutant complexed with CoA is shown in Figure 2A. The final models included residues Met1−Ile389 in the C164A mutant, Val2−Ile389 in the H303Q mutant, and Ser3−Ile389 in the N336A mutant. Electron density for CoA was apparent in the N336A mutant. In addition, a sulfate molecule was modeled near the side-chain hydroxyl group of Ser5 and the backbone nitrogens of Val4 and Ser5 in each structure, and a bis-Tris-propane molecule was modeled in the CoA-binding tunnel of the C164A mutant.

The structure of the C164A mutant shows that minimal changes were introduced at the active site (Figure 7a). His303 and Asn336 maintain their positions in the active site because of a network of hydrogen bond interactions that is nearly identical to that observed in the wild-type enzyme (Figure 8). This network includes two water molecules found on the side of His303 distal to the active site. The structure of the H303Q mutant revealed that substitution of glutamine for His303 resulted in only slight perturbations at the active site (Figure 7B). This structure demonstrates that the hydrogen-bonding ability of the N_ϵ of His303 is retained by the amide nitrogen of Gln303, as suggested by kinetic analysis of this mutant. Likewise, comparison of the N336A mutant and wild-type CHS structures shows that replacement of Asn336 with an alanine introduced few changes at the active site (Figure 7C). The only major difference is that the methyl group of Ala336 allows an additional water molecule into the active site; this water interacts with the N_ϵ of His303 (2.9 Å) and the S_γ of Cys164 (3.4 Å).

The N336A structure revealed that CoA binds to the mutant enzyme in a conformation analogous to that observed in the wild-type CHS·CoA complex (Figure 7D). Although van der Waals contacts dominate the protein−ligand interactions, Lys55 and Arg58 interact with the phosphate on the ribose group and Lys62 hydrogen bonds with the phosphate nearest the ribose on the diphosphate bridge to the pantetheine arm. Interaction between the backbone amide of Ala308 and the carbonyl oxygen of the pantetheine arm forms the final hydrogen bond between CHS and CoA.

The structures of these mutants demonstrate the flexibility of Phe215 and Ph265. In both the C164A and N336A mutant structures, Phe215's benzyl moiety rotates about the χ_2 angle from the conformation seen in the wild-type and H303Q mutant structures and Phe265's benzyl group rotates into the cyclization pocket in both of these mutants. This rearrangement of Phe265 may depend on occupancy of the CoA-binding site, since a bis-Tris propane molecule is bound in the C164A mutant and a CoA molecule in the N336A mutant. Comparison of the structure of CHS complexed with CoA and the N336A mutant (Figure 7D) suggests that the position of the CoA's terminal thiol may influence the conformations of Phe215 and Phe265.

DISCUSSION

Cys164 Serves as the Nucleophile for Polyketide Formation and Is Not Essential for Malonyl-CoA Decarboxylation. Our results confirm the role of Cys164 as the nucleophile that initiates the reaction and as the attachment site for the enzyme-bound polyketide intermediates required for chalcone formation (*6*, *19*). Although replacement of Cys164 with an alanine eliminates the nucleophile required for covalent attachment of polyketide reaction intermediates to CHS (*7*, *19*), the C164A mutant still catalyzes malonyl-CoA decarboxylation. Supporting our finding that Cys164 is not essential for the decarboxylation reaction, previous studies of parsley CHS demonstrated that the thiol-specific compounds iodoacetate and iodoacetamide did not inhibit malonyl-CoA decarboxylation (*20*). Thus, the active-site residues responsible for the decarboxylation reaction reside elsewhere in the CHS active site and likely include His303 and Asn336, as discussed below.

A number of fatty acid synthases catalyze decarboxylation reactions without the active-site thiol being occupied by an enzyme-bound intermediate but at less than 25% of the product formation rate (*50*−*52*). In addition, substitutions of the active-site cysteine in the structurally homologous KAS II eliminate the condensation reaction but conserve decarboxylase activity (*53*). Unlike these examples, CHS

catalyzes the decarboxylation of malonyl-CoA with a rate similar to that of chalcone formation. It is possible that the true decarboxylation rate of CHS is different from that determined here, since the enzyme state in the measured malonyl-CoA decarboxylation reaction (free Cys164) does not resemble that normally occurring during chalcone formation, i.e., a polyketide intermediate covalently attached at Cys164. Indeed, suitable mimics of each of the four structurally distinct enzyme−ketide intermediates would be necessary to unravel the decarboxylation rates during each of the malonyl-CoA decarboxylation steps.

Role of His303 in Chalcone Formation and Malonyl-CoA Decarboxylation. In the structure of CHS, His303 is within hydrogen-bonding distance of Cys164 (*22*). This interaction initially suggested that the histidine could abstract a proton from Cys164 to form the reactive thiolate necessary for initiation and polyketide elongation. Our results demonstrate that the H303Q mutant retains nearly all wild-type activity with only a 10-fold reduction in the turnover rate for chalcone formation. This decrease is inconsistent with the 100−1000-fold reduction in turnover rate usually associated with the loss of a general base in an enzymatic mechanism (*54*, *55*). However, the loss of a stable thiolate-imidazolium ion pair at the CHS active site resembling that of the cysteine proteases could explain the small changes in turnover rate (*56*).

The substitution of His303 with a glutamine residue is a structurally isosteric substitution as the amide nitrogen of the Gln303 side chain still forms a hydrogen bond with Cys164. This interaction may sufficiently perturb the pK_a of the cysteine to allow generation of the thiolate required for initiating chalcone formation with the reduced turnover rate reflecting the energetic loss of going from a charge−charge (imidazole-thiolate) pair to a neutral-charge (amide-thiolate) pair at the active site. Alternatively, the greater degrees of freedom accessible to glutamine versus histidine at position 303 may result in a slightly diminished turnover rate. Further experiments, including assignment of microscopic pK_a values to determine if an imidazolium-thiolate ion pair is present at the CHS active site, must be performed.

Our results also indicate that His303 plays a key role in the decarboxylation of malonyl-CoA. First, of the His303 mutants examined, only the H303Q mutant remains active during malonyl-CoA decarboxylation with a modest reduction in turnover rate for malonyl-CoA decarboxylation. Second, in the three-dimensional structures of the C164A mutant and the previously described C164S mutant (*22*) His303 remains in the same position as in wild-type CHS. Together with the crystal structure of the H303Q mutant, it is clear that each of these mutants retains the capacity for hydrogen bonding with the thioester carbonyl of malonyl-CoA. This interaction likely promotes formation of an oxyanion hole near the carbonyl oxygen of the acetyl anion during the decarboxylation reaction.

In a number of enzymatic and nonenzymatic systems, a positive charge is used to stabilize an enolate produced during a decarboxylation reaction (*57*−*65*). In CHS, an imidazolium ion at position 303 would be mechanistically useful, since a positive charge on His303 could stabilize the developing negative charge on the thioester carbonyl of malonyl-CoA and lower the energy barrier during the transition state for the decarboxylation reaction. A similar role has been proposed for a lysine residue in fatty acid synthase in which a positive charge acts as an electron sink to stabilize formation of the acetyl-carbanion required for the condensation reaction by a non-Schiff base mechanism (*66*, *67*). Nevertheless, the kinetic results obtained for the H303Q mutant clearly demonstrate that the loss of a potential positive charge at position 303 results in only a modest reduction in both decarboxylation activity and the rate of chalcone formation. Therefore, hydrogen bonding to the thioester carbonyl oxygen is a key interaction necessary for both activities in CHS.

Asn336 as the Second Component of the Decarboxylation Machinery. Characterization of the Asn336 mutants suggests that this residue interacts with substrates during the formation of chalcone and potentially stabilizes the transition state during malonyl-CoA decarboxylation. First, the K_d values for CoA and acetyl-CoA binding of the Asn336 mutants indicates that the amide side chain may interact with the carbonyl of acetyl-CoA. Second, the k_{cat}/K_m values for malonyl-CoA versus coumaroyl-CoA in naringenin formation suggest that mutation of Asn336 impacts mainly upon the malonyl-CoA portion of the reaction. Third, a hydrogen bond was observed between Asn336's side-chain amide and the thioester carbonyl of bound hexanoyl-CoA in a previously described C164S mutant structure (*22*). It is likely that an analogous interaction occurs upon binding of coumaroyl- and malonyl-CoA.

The Asn336 mutants demonstrate that substrate binding is not sufficient for catalysis in CHS. For example, the N336Q and N336H mutants bind acetyl-CoA with 40- and 2-fold increases in the K_d value over wild-type CHS, respectively, but neither catalyzes malonyl-CoA decarboxylation, while the N336A and N336D mutants exhibit similar differences of the K_d values for acetyl-CoA binding and both catalyze the decarboxylation reaction. Together these results suggest that binding of malonyl-CoA (and potentially coumaroyl-CoA) in a catalytically optimal conformation requires hydrogen bonding between the thioester carbonyl of substrates and the side-chain amide of Asn336.

The participation of Asn336 in orienting malonyl-CoA at the active site would provide an interaction that facilitates the decarboxylation reaction. However, the N336A, N336D, and N336K mutants compromise this interaction, as these enzymes catalyze the decarboxylation reaction with substantial decreases in catalytic efficiency. As determined crystallographically, the N336A mutant eliminates any potential interaction between position 336 and the substrate or reaction intermediates without disturbing the positions of Cys164 and His303. Our results also suggest that without the guiding interaction of Asn336, malonyl-CoA may sample a range of conformations at the CHS active site, only some of which allow interaction with His303 and the decarboxylation reaction to proceed. This is based on the drastic differences in the catalytic efficiencies for coumaroyl-CoA and malonyl-CoA exhibited by the Asn336 mutants. The use of binding interactions for orienting substrates at an enzyme active site is documented in a number of systems, in which the proper position of substrates at the active site permits "catalytic" residues to exert their maximal effect, thereby linking the contribution of binding interactions to catalysis (*68*−*79*). Therefore, we conclude that the hydrogen bond between Asn336 and the thioester carbonyl of malonyl-CoA ensures the proper conformation for decarboxylation and for subse-

quent condensation of the acetyl carbanion to the enzyme-bound polyketide intermediate.

Proposed Role for Phe215. On the basis of the crystal structure of CHS (*22*), Phe215 was proposed to interact with acyl-CoA substrates through van der Waals contacts. Neither the F215S mutant nor the F215Y mutant significantly alters the K_d for CoA or acetyl-CoA binding, but each dramatically alters the turnover rates for malonyl-CoA decarboxylation and chalcone formation. During the decarboxylation reaction, Phe215 may orient the terminal carboxylate of malonyl-CoA through van der Waals interactions. Additionally, as conversion of a carboxylate group, which is polar and charged, into carbon dioxide, which is nonpolar and uncharged, is sensitive to environment (*57*), Phe215 could provide a nonpolar environment that favors the decarboxylation of malonyl-CoA. Furthermore, the increased proportion of truncated reaction products observed in reactions catalyzed by the Phe215 mutants indicates that the substitutions at position 215 may interfere with elongation of the polyketide intermediate.

Reaction Sequence for CHS. We now present a modified reaction mechanism for chalcone formation catalyzed by CHS. Binding of *p*-coumaroyl-CoA initiates the reaction. The thiolate of Cys164 attacks the thioester carbonyl, resulting in transfer of the coumaroyl moiety to the cysteine side chain (Figure 9a, R = coumaroyl). Asn336 hydrogen bonds with the thioester carbonyl, further stabilizing formation of the tetrahedral reaction intermediate. CoA then dissociates from the enzyme, leaving a coumaroyl-thioester at Cys164. Malonyl-CoA binds and positions the bridging carbon of the malonyl moiety near the carbonyl of the enzyme-bound coumaroyl thioester. Asn336 orients the thioester carbonyl of malonyl-CoA near His303 with Phe215, providing a nonpolar environment for the terminal carboxylate that facilitates decarboxylation. His303 and Asn336 interact with the substrate's thioester carbonyl, creating an efficient electron sink or oxyanion hole that stabilizes the developing negative charge during the decarboxylation step through stabilization of the enol tautomer of the acetyl anion (Figure 9B). Moreover, the presence of a stabilized anion also reduces its reactivity toward CO_2, thereby driving the reaction forward. Attack of the carbanion on the carbonyl of the enzyme-bound coumaroyl thioester releases the thiolate anion of Cys164 and transfers the coumaroyl group to the acetyl moiety of the CoA thioester (Figure 9C). Hydrogen bonds from His303 and Asn336 would stabilize the tetrahedral transition state of this reaction. Recapture of the elongated coumaroyl-acetyl-diketide-CoA by Cys164 and release of CoA set the stage for two additional rounds of elongation, resulting in formation of the final tetraketide reaction intermediate.

It is unclear whether generation of the carbanion and formation of the elongated ketide intermediates occur as distinct or concerted reactions. The apparent lack of enzyme-catalyzed proton exchange with solvent for thiolase and the *E. coli* condensing enzymes may support a concerted reaction (*80*, *81*). However, similar observations were made for malate synthase, but its reaction occurs in two steps using a formal carbanion intermediate (*82*). Likewise, modeling of the decarboxylation and condensation reactions of fatty acid synthase suggests that decarboxylation of the malonyl group occurs before condensation of the resulting anion without protonation of the reaction intermediate (*66*).

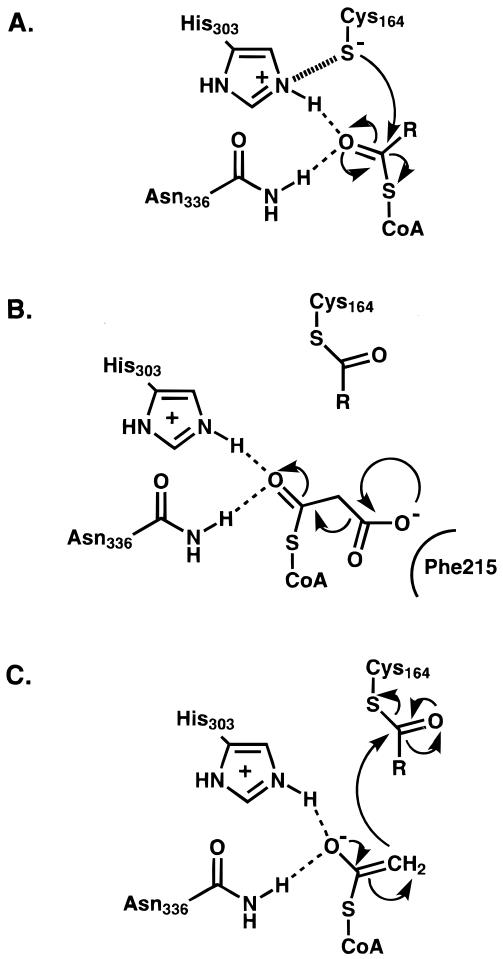

FIGURE 9: Reaction mechanism of decarboxylation and chalcone formation catalyzed by CHS. (A) Transfer of the starter coumaroyl (R) from CoA to Cys164. (B) Decarboxylation of malonyl-CoA is catalyzed by His303 and Asn336. The proposed role of Phe215 in orienting the terminal carboxylate of malonyl-CoA is diagrammed schematically. R for this step ranges from coumaroyl- to the penultimate triketide intermediate. (C) Resonance of the enolate ion to the keto form allows for condensation of the acetyl carbanion with the enzyme-bound polyketide intermediate.

The final step in chalcone formation involves an intramolecular Claisen condensation encompassing the three acetate units derived from three malonyl-CoAs. During cyclization, the nucleophilic methylene group nearest the coumaroyl moiety attacks the carbonyl carbon of the thioester linked to Cys164. Ring closure is proposed to proceed through an internal proton transfer from the nucleophilic carbon to the carbonyl oxygen. Breakdown of this tetrahedral intermediate expels the newly cyclized ring system from Cys164. Subsequent aromatization of the trione ring through a second series of facile internal proton transfers yields chalcone.

Relationship of the CHS Mechanism to That of β-Ketoacyl Synthase (KAS) II. The roles of Cys164, His303, and Asn336 in catalysis may be similar in other KAS modules of the more complex polyketide and fatty acid synthases. Structurally, these three residues in CHS are analogous to Cys163, His303, and His340 of KAS II from *E. coli* (*23*), which catalyzes the addition of acetate to palmoleitic acid. Unlike CHS, this enzyme uses an acyl carrier protein instead of a CoA thioester to shuttle substrates to the active site. Recent work has demonstrated that the active-site cysteine of KAS II is not required for decarboxylase activity (*53*). Huang et

al. (*23*) proposed roles for the two histidines of KAS II that are the opposite from those suggested for the active-site histidine and asparagine of CHS. In the KAS II crystal structure, His340 is closer to the S_γ atom of the active-site cysteine than is His303. In CHS, His303 is closer to the active-site cysteine than is Asn336. On the basis of these observations, His340 in KAS II may stabilize the nucleophilic thiolate with His303 of KAS II aiding in binding the second substrate at the active site by guiding the C2 carbon of the acetyl-acyl carrier protein into position for the condensation step. In addition, both the histidines of the KAS II active site could stabilize the transition state of the decarboxylation reaction. These differences at the active site of KAS II may also reflect the need to accommodate a slightly different position of the malonyl substrate that results from using an acyl-carrier protein instead of a CoA thioester.

Conclusions. All polyketide and fatty acid synthases catalyze a common condensation reaction in which an acyl−enzyme intermediate undergoes nucleophilic attack by a carbanion derived from a decarboxylation reaction. CHS and the related polyketide synthases, including STS, BBS, ACS, and 2-PS, use a single active site containing four conserved amino acids to perform a series of decarboxylation, condensation, cyclization, and aromatization reactions (*6*). The results of this study, and the structural similarity of CHS to KAS II, suggest that a common set of active-site features exists across the family of polyketide and fatty acid synthases, implying evolutionarily conserved mechanistic features (*83*). Further studies focused on how polyketide synthases, like CHS, control the choice of starter molecule, the number of acetate additions, and the stereochemistry of the cyclization reaction will shed further light on the mechanism of these enzymes.

REFERENCES

1. Hopwood, D. A. (1997) *Chem. Rev. 97*, 2465−2497.
2. Cane, D. E., Walsh, C. T., and Khosla, C. (1998) *Science 282*, 63−68.
3. Donadio, S., Staver, M. J., McAlpine, J. B., Swanson, S. J., and Katz, L. (1991) *Science 252*, 675−679.
4. Kreuzaler, F., Ragg, H., Heller, W., Tesch, R., Witt, I., Hammer, D., and Hahlbrock, K. (1979) *Eur. J. Biochem. 99*, 89−96.
5. Tropf, S., Kärcher, B., Schröder, G., and Schröder, J. (1995) *J. Biol. Chem. 270*, 7922−7928.
6. Preisig-Müller, R., Gehlert, R., Melchior, F., Stietz, U., and Kindl, H. (1997) *Biochemistry 36*, 8349−8358.
7. Schröder, J. (1997) *Trend Plant Sci. 2*, 373−378.
8. Bailey, J. A., and Mansfield, J. W. (1982) *Phytoalexins*, John Wiley and Sons, NY.
9. Long, S. R. (1989) *Cell 56*, 203-214.
10. Dixon, R. A., and Paiva, N. L. (1995) *Plant Cell 7*, 1085−1097.
11. Edwards, M. L., Stemerick, D. M., and Sunkara, P. S. (1990) *J. Med. Chem. 33*, 1948−1954.
12. Li, R., Kenyon, G. L., Cohen, F. E., Chen, X., Gong, B., Dominguez, J. N., Davidson, E., Kurzban, G., Miller, R. E., Nuzum, E. O., Rosenthal, P. J., and McKerrow, J. H. (1995) *J. Med. Chem. 38*, 5031−5037.
13. Zwaagstra, M. E., Timmerman, H., Tamura, M., Tohma, T., Wada, Y., Onogi, K., and Zhang, M.-Q. (1997) *J. Med. Chem. 40*, 1075−1089.
14. Gehm, B. D., McAndrews, J. M., Chien, P.-Y., and Jameson, J. L. (1997) *Proc. Natl. Acad. Sci. U.S.A. 94*, 14138−14143.
15. Jang, M., Cai, L., Udeani, G. O., Slowing, K. V., Thomas, C. F., Beecher, C. W. W., Fong, H. H. S., Farnsworth, N. R., Kinghorn, A. D., Mehta, R. G., Moon, R. C., Pezzuto, J. M. (1997) *Science 275*, 218−220.
16. Frankel, E. N., Kanner, J., German, J. B., Parks, E., and Kinsella, J. E. (1993) *Lancet 341*, 454−457.
17. Frankel, E. N., Waterhouse, A. L., and Kinsella, J. E. (1993) *Lancet 341*, 1103−1104.
18. Kreuzaler, F., and Hahlbrock, K. (1975) *Eur. J. Biochem. 56*, 205−213.
19. Lanz, T., Tropf, S., Marner, F.-J., Schröder, J., and Schröder, G. (1991) *J. Biol. Chem. 266*, 9971−9976.
20. Kreuzaler, F., Light, R. J., and Hahlbrock, K. (1978) *FEBS Lett. 94*, 175−178.
21. Hahlbrock, K., Zilg, H., and Grisebach, H. (1970) *Eur. J. Biochem. 15*, 13−18.
22. Ferrer, J.-L., Jez, J. M., Bowman, M. E., Dixon, R. A., and Noel, J. P. (1999) *Nat. Struct. Biol. 6*, 775−784.
23. Huang, W., Jia, J., Edwards, P., Dehesh, K., Schneider, G., and Lindqvist, Y. (1998) *EMBO J. 17*, 1183−1191.
24. Mathieu, M., Zeelen, J. P., Pauptit, R. A., Erdmann, R., Kunau, W.-H., and Wierenga, R. K. (1994) *Structure 2*, 797−808.
25. Schröder, G., Brown, J. W. S., and Schröder, J. (1988) *Eur. J. Biochem. 172*, 161−169.
26. Preisig-Müller, R., Gnau, P., and Kindl, H. (1995) *Arch. Biochem. Biophys. 317*, 201−207.
27. Junghanns, K. T., Kneusel, R. E., Baumert, A., Maier, W., Groger, D., and Matern, U. (1995) *Plant Mol. Biol. 27*, 681−692.
28. Helaruitta, Y., Kotilainen, M., Elomaa, P., Kalkkinen, N., Bremer, K., Teeri, T. H., and Albert, V. A. (1996) *Proc. Natl. Acad. Sci. U.S.A. 93*, 9033−9038.
29. Thomashow, L. S., and Bangera, M. G. (1995) GenBank submission.
30. Sorokin, A., Azevedo, V., Zumstein, E., Galleron, N., Ehrlich, S. D., and Serror, P. (1996) *Microbiology 142*, 2005−2016.
31. Cole, S. T., et al. (1998) *Nature 393*, 537−544.
32. Junghans, H., Dalkin, K., and Dixon, R. A. (1993) *Plant Mol. Biol. 22*, 239−253.
33. Stoeckigt, J., and Zenk, M. H. (1975) *Z. Naturforsch. 30c*, 352−358.
34. Eckermann, S., Schröder, G., Schmidt, J., Strack, D., Edrada, R. A., Helariutta, Y., Elomaa, P., Kotilainen, M., Kilpeläinen, I., Proksch, P., Teeri, T. H., and Schröder, J. (1998) *Nature 396*, 387−390.
35. Fersht, A. (1985) *Enzyme Structure and Mechanism*, W. H. Freeman and Company, New York.
36. Otwinowski, Z., and Minor, W. (1997) *Methods Enzymol. 276*, 307−326.
37. Collaborative Computational Project 4 (CCP4) (1994) *Acta Crystallogr., Sect. D 50*, 760−763.
38. Ten Eyck, L. F. (1973) *Acta Crystallogr., Sect. A 29*, 183−191.
39. Ten Eyck, L. F. (1977) *Acta Crystallogr., Sect. A 33*, 486-492.
40. Murshudov, G. N., Vagin, A. A., and Dodson, E. J. (1997) *Acta Crystallogr., Sect. D 53*, 240−255.
41. Lamzin, V. S., and Wilson, K. S. (1993) *Acta Crystallogr., Sect. D 49*, 129−147.
42. Jones, T. A., Zou, J. Y., Cowan, S. W., and Kjeldgaard, M. (1993) *Acta Crystallogr., Sect. D 49*, 148−157.
43. Laskowski, R. A., MacArthur, M. W., Moss, D. S., and Thornton, J. M. (1993) *J. Appl. Crystallogr. 26*, 283−291.
44. Kreuzaler, F., and Hahlbrock, K. (1975) *Arch. Biochem. Biophys. 169*, 84−90.
45. Hrazdina, G., Kreuzaler, F., Hahlbrock, K., and Grisebach, H. (1976) *Arch. Biochem. Biophys. 175*, 392−399.
46. Palmer, M. A. J., Differding, E., Gamboni, R., Williams, S. F., Peoples, O. P., Walsh, C. T., Sinskey, A. J., and Masamune, S. (1991) *J. Biol. Chem. 266*, 8369−8375.
47. Schüz, R., Heller, W., and Hahlbrock, K. (1983) *J. Biol. Chem. 258*, 6730−6734.
48. Schröder, J., Raiber, S., Berger, T., Schmidt, A., Schmidt, J., Soares-Sello, A. M., Bardshiri, E., Strack, D., Simpson, J., Veit, M., and Schröder, G. (1998) *Biochemistry 37*, 8417−8425.

49. Schöppner, A., and Kindl, H. (1984) *J. Biol. Chem. 259*, 6806−6811.
50. Smith, S., and Abraham, S. (1970) *J. Biol. Chem. 245*, 3209−3217.
51. Kresze, G. B., Steber, L., Oesterhelt, D., and Lynen, F. (1977) *Eur. J. Biochem. 79*, 181−90.
52. Srinivasan, K. R., and Kumar, S. (1981) *Biochemistry 20*, 3400−3404.
53. Witkowski, A., Joshi, A. K., Lindqvist, Y., and Smith, S. (1999) *Biochemistry 38*, 11643−11650
54. Jencks, W. P. (1969) *Catalysis in Chemistry and Enzymology*, McGraw-Hill, NY.
55. Carter, P., and Wells, J. A. (1988) *Nature 332*, 564−568.
56. Storer, A. C., and Menard, R. (1994) *Methods Enzymol. 244*, 486-500.
57. O'Leary, M. H. (1992) in *The Enzymes* (Sigman, D. S., and Boyer, P. D., Eds.) Vol. 20, pp 235−269, Academic Press, New York.
58. Steinberger, R., and Westheimer, F. H. (1951) *J. Am. Chem. Soc. 73*, 429−435.
59. Raghaven, N. V., and Leussing, D. L. (1976) *J. Am. Chem. Soc. 98*, 723−730.
60. Miller, B. A., and Leussing, D. L. (1985) *J. Am. Chem. Soc. 107*, 7146−7153.
61. Loken, J. P., and Stormer, F. C. (1970) *Eur. J. Biochem. 14*, 133−137.
62. Hermes, J. D., Tipton, P. A., Fisher, M. A., O'Leary, M. H., Morrison, J. F., and Cleland, W. W. (1984) *Biochemistry 23*, 6263−6275.
63. Rendina, A. R., Hermes, J. D., and Cleland, W. W. (1984) *Biochemistry 23*, 6257−6262.
64. Ankel, H., and Feingold, D. S. (1965) *Biochemistry 4*, 2468−2475.
65. Ankel, H., and Feingold, D. S. (1966) *Biochemistry 5*, 182−189.
66. Dewar, M. J. S., and Dieter, K. M. (1988) *Biochemistry 27*, 3302−3308.
67. Stoops, J. K., Henry, S. J., and Wakil, S. J. (1983) *J. Biol. Chem. 258*, 12482−12486.
68. Storm, D. R., and Koshland, D. E. (1970) *Proc. Natl. Acad. Sci. U.S.A. 66*, 445−452.
69. Milstein, S., and Cohen, L. A. (1970) *Proc. Natl. Acad. Sci. U.S.A. 67*, 1143−1147.
70. Nowak, T., and Mildvan, A. S. (1972) *Biochemistry 11*, 2813−2818.
71. Jencks, W. P., and Page M. I. (1974) *Biochem. Biophys. Res. Commun. 57*, 887−892.
72. Jencks, W. P. (1975) *Adv. Enzymol. 43*, 219−410.
73. Bruice, T. C. (1970) in *The Enzymes* (Boyer, P. D., Ed.) Vol. 2, pp 217−279, Academic Press, New York.
74. Fersht, A. R. (1987) *Biochemistry 26*, 8031−8037.
75. Bohren, K. M., Grimshaw, C. E., Lai, C. J., Harrison, D. H., Ringe, D., Petsko, G. A., and Gabbay, K. H. (1994) *Biochemistry 33*, 2021−2032.
76. Cannon, W. R., Singleton, S. F., and Benkovic, S. J. (1996) *Nat. Struct. Biol. 3*, 821−833.
77. Jez, J. M., and Penning, T. M. (1998) *Biochemistry 37*, 9696−9703.
78. Narlikar, G. J., and Herschlag, D. (1998) *Biochemistry 37*, 9902−9911.
79. Menger, F. M. (1992) *Biochemistry 31*, 5368−5373.
80. Davis, J. T., Moore, R. N., Imperali, B., Pratt, A. J., Kobayashi, K., Masamune, S., Sinskey, A. J., and Walsh, C. T. (1987) *J. Biol. Chem. 262*, 82−89.
81. Arnstadt, K. I., Schindlbeck, G., and Lynen, F. (1975) *Eur. J. Biochem. 55*, 561−571.
82. Clark, J. D., O'Keefe, S. J., and Knowles, J. R. (1988) *Biochemistry 27*, 5961−5971.
83. Siggaard-Andersen, M. (1993) *Protein Seq. Data Anal. 5*, 325−335.
84. Brunger, A. T. (1992) *Nature 355*, 472−475.
85. Kraulis, P. J. (1991) *J. Appl. Crystallogr. 24*, 946−950.
86. POV-Team (1997) *POV-Ray: Persistence of vision raytracer.*

BI991489F